JOURNAL OF MATERIALS SCIENCE 23 (1988) 946–957

Effect of particulate additions on the contact damage resistance of hot-pressed Si_3N_4

R. A. PAGE, C. R. BLANCHARD-ARDID, W. WEI
Southwest Research Institute, San Antonio, Texas 78284, USA

Silicon nitride matrix composites containing particles of SiC, TiC, and BN were fabricated and tested for improved contact damage resistance at 900° C in an oxidizing atmosphere. Contact damage resistance was characterized with profilometry, scanning electron microscopy, bend tests, and coefficient of friction measurements. The results of these tests indicated that composites containing TiC particles showed dramatically improved friction and wear behaviour compared to the SiC- and BN-containing composites, as well as the monolithic Si_3N_4. Auger spectroscopy indicated that the improved behaviour was due to the formation of a lubricious oxide containing both titanium and silicon on the surface of the composite and the transfer of some of the oxide to the rider.

1. Introduction

The modern gas turbine engine is an archetypal example of the technological limitations imposed by the attainable properties of currently available engineering materials. The performance of these engines is dependent on the attainment of extremely high operating temperatures. Also, in addition to the obvious desirability of a high thrust-to-weight ratio, the multiplication in applied stress induced by the self-loading of rotating components requires that the weight of such components be minimized. Superalloys, even with the most modern alloys and advanced processing techniques, are limited to continuous service at temperatures below 1150° C. Additionally, the strength-to-density ratio for the nickel- and cobalt-based superalloys is quite low.

It is apparent that, in order to achieve significant improvements in engine operating temperatures and weight, an entirely new class of materials must be employed. Although the potential of ceramic materials for this application has been recognized for some time, the transition from metals to ceramics has been impeded by a number of serious obstacles, such as the low fracture toughness and thermal shock resistance and the poor property reproducibility in parts fabricated in complex shapes. Recent advances in the technology of ceramic materials have demonstrated the potential for overcoming many of these problems and have spurred a resurgence of interest in ceramics as structural materials.

Although a great deal of effort has been expended on understanding and improving the tensile strength, toughness, and thermal shock resistance of ceramic materials, very little is known about the technologically important area of contact damage. Recent programmes which have attempted to produce ceramic engine components have experienced numerous catastrophic failures which have been attributed to contact damage [1–3]. This type of damage, which is manifested in the form of small flaws which severely degrade strength, results from concentrated loading at small contact areas between the ceramics and other hard components. The localized contact stresses responsible for the surface damage arise from design tolerances which lead to abnormal contact of mating components and contact sliding induced by thermal expansion. Vibrational loading may also contribute to the contact damage. An interesting aspect of this observation is that contact damage due to oscillatory sliding, or fretting, may differ in nature from that induced by a single sliding contact in one direction only. This fretting damage is of particular concern in the blade attachment region of ceramic turbine blades [3].

Certain aspects of contact damage in brittle materials are well described by current theories. Fracture around microhardness indentations, formed by quasi-static loads applied normal to the material surface, has been the subject of extensive mathematical analyses and numerous experimental verifications [4–7]. In fact, the process of cracking under normal loading is well enough understood that normal indentations are now routinely used to obtain estimates of fracture toughness [4, 8] and to introduce well-defined flaws into fracture mechanics specimens [9].

The most serious contact damage in ceramic components seems to result not from normal contact forces, but from contact with a sliding surface. During sliding contact, the tensile stresses which arise at the trailing edge of a sliding contact due to frictional forces facilitate the formation of partial cone cracks [10, 11]. Under the influence of a sliding surface, the critical normal load for crack initiation is reduced by a factor which contains the coefficient of friction raised to a power ranging from 1.5 [10] to 3.0 [12]. Thus, the coefficient of friction plays a major role in determining the susceptibility of a ceramic material to contact damage. Other material parameters which would be expected to influence susceptibility to contact damage are fracture toughness and hardness.

0022–2461/88 $03.00 + .12

This paper presents the results of a study designed to determine what improvement in contact damage resistance could be obtained by the addition of various ceramic particulates to a silicon nitride matrix. The particulates were chosen so as to vary the fracture toughness, hardness and coefficient of friction, which are thought to be three of the primary material parameters controlling contact damage.

2. Experimental procedures

2.1. Material fabrication

A hot-pressed monolithic ceramic of Si_3N_4 + 6% CeO_2 served as the baseline material for this study. Composites were formed by the addition of 20 vol % of either SiC, TiC, or BN particles to the baseline material. The powders used for fabrication included α-Si_3N_4 (Grade LC12, Hermann C. Starck, Inc., New York) with 0.55 μm average particle size, α-SiC (Starck Grade A10) with 1.25 μm average particle size, TiC (Starck c.a.s. grade) with 1.25 μm average particle size, BN (99.5% pure, Cerac Inc., Milwaukee) with 1 μm average particle size, and CeO_2 (Cerac 99.9% pure). Mixtures of the proper compositions were wet ball-milled for 24 h with Al_2O_3 balls in n-hexane in polyethylene jars prior to hot-pressing.

Billets 6.35 cm in diameter and 0.6 to 0.8 cm thick were uniaxially hot-pressed in a filament-wound graphite die lined with Grafoil (Carbon Products Division, Union Carbide Corp., Chicago). The hot-pressing schedule, which was similar to that employed by Mazdiyasni and Ruh [13], consisted of an initial cold-pressing to 34.5 MPa, pressureless heating to 1200° C, loading to 34.5 MPa and heating rapidly to 1800° C, then holding for 3 h at 1800° C. Following the 3 h hold, the samples were cooled slowly to room temperature under load. In order to minimize reduction of the Si_3N_4, the entire hot-pressing procedure was performed in a nitrogen atmosphere. The above procedures produced compacts with densities ranging from 94 to 97% of theoretical.

2.2. Material characterization

Following fabrication, the density, hardness, fracture toughness, modulus of rupture and Young's modulus were measured for each of the as-hot-pressed materials. The densities were determined by the Archimedes method. Flexural strengths are obtained from 5.08 cm long × 0.635 cm wide × 0.318 cm thick samples tested on a self-aligning four-point bend apparatus with a major span of 4.44 cm and a minor span of 2.22 cm. Young's moduli were obtained from strain-gauged four-point bend specimens. Hardness and fracture toughness were determined simultaneously from diamond pyramid indentations. For these tests, polished surfaces cut parallel to the hot-pressing direction were indented with a diamond pyramid indenter using a 10 kg load. The indenter was oriented such that one axis was parallel and the other axis was perpendicular to the hot-pressing direction. Hardness values, H, were calculated from

$$H = P/2a^2 \quad (1)$$

where P is the indentation load and $2a$ is the width of the indentation. Fracture toughness values, K_{Ic}, were calculated [11] from

$$\left(\frac{K_{Ic}\phi}{Ha^{1/2}}\right)\left(\frac{H}{E\phi}\right)^{0.4} = 0.129\left(\frac{c}{a}\right)^{-3/2} \quad (2)$$

where E is Young's modulus, $2c$ is the crack length and ϕ is a constant equal to 3. With the exception of the BN composite, for which no cracks were observed parallel to the hot-pressing direction, indentation with a 10 kg load produced cracks which satisfied the condition $c/a \geqslant 2$.

2.3. Contact damage resistance evaluation

A schematic illustration of the specialized high-temperature friction and wear test rig in which the contact damage resistance of the various materials was evaluated is shown in Fig. 1. The specimen configuration involved a ceramic flexural test bar (dimensions described previously) that oscillated its tensile surface against a stationary 0.63 cm hemisphere of sintered α-SiC (The Carborundum Company, Research and Development Division, Niagara Falls, New York). A controlled normal load was applied through the lever arm holding the hemispherical pin. The tangential force applied to the pin was measured continuously using a calibrated strain gauge bridge, strain indicator, and strip chart recorder. The coefficient of friction, μ_f, was calculated by dividing the measured tangential force by the applied normal force. Heating was supplied by resistance elements insulated in ceramic fibre which surrounded the pin and test bar. The temperature was controlled by a thermocouple attached to the lever arm with the junction 2.5 cm from the ceramic hemisphere.

For the single-stroke test, a variation of the testing rig was necessary. Rather than using a motor-driven eccentric as the source of the tangential force on the specimen, a gradually increasing load was employed. This enabled the measurement of the load needed for pin breakaway and the calculation of the static coefficient of friction.

Table I lists the three test conditions used in the friction and wear experiments. At least two specimens of each material were tested under each of the three conditions. All experiments were run non-lubricated in air at 900° C. The testing times for the oscillating experiments were 1 or 15 min with normal loads of 14.7 or 4.9 N, respectively. The stroke length of the pin on flat for all tests was 2.0 cm. The single-stroke experiments employed an increasing tangential force until movement commenced, allowing for a relatively constant velocity with a normal load of 4.9 N.

Operating under the assumption that partial cone cracks were the primary form of damage produced during sliding contact, the resistance of the materials to this type of damage was evaluated by measuring the residual bend strengths of the wear bars. To maximize the possibility of detecting the presence of any cracking, the partial cone cracks were aligned for maximum tensile loading in the four-point bend tests, i.e. the wear track was situated on the tensile surface and parallel to the tensile stress axis. The presence of

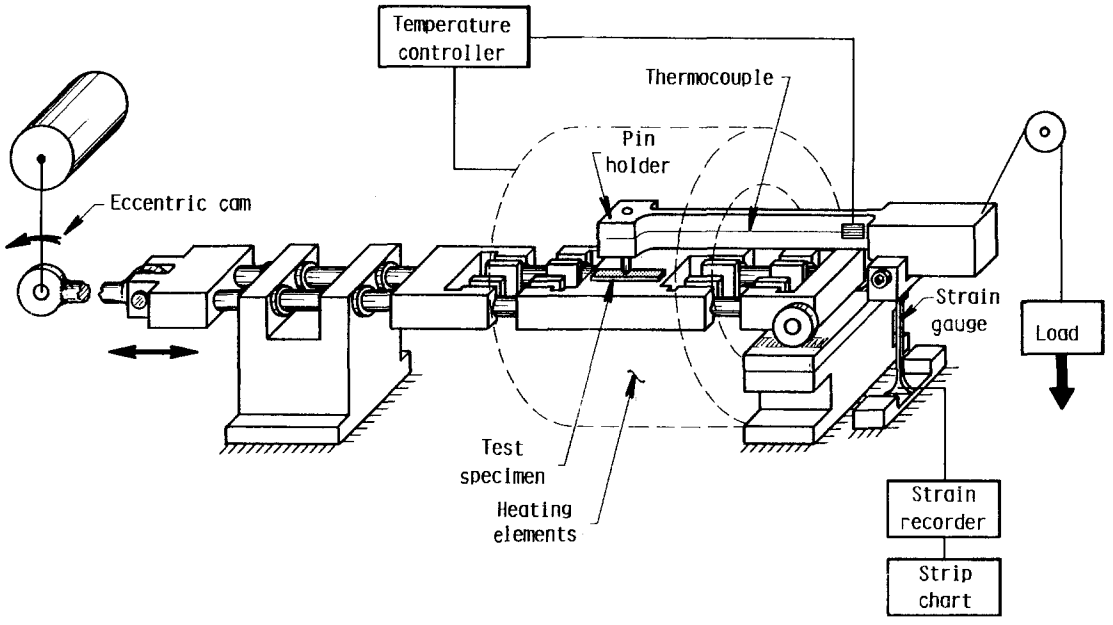

Figure 1 Schematic diagram of specialized friction and wear apparatus.

damage would thus manifest itself as a reduction in flexural strength compared to as-hot-pressed values. Additional characterization included profilometer measurements and microscopic examination across the wear tracks, characterization of the cracking within the wear tracks, and Auger analysis of the pins and wear tracks.

3. Results

3.1. As-fabricated properties

The processing procedures described above produced compacts ranging in density from 94.26 to 96.90% of theoretical with a fairly uniform distribution of the particulate additions. The as-fabricated properties of the hot-pressed materials are listed in Table II. The flexural strength listed in the table represents the average of from five to seven bend-bars. The hardness and fracture toughness values represent averages obtained on ten indents. The indents were placed such that one set of cracks propagated along the hot-pressing direction while the second set propagated perpendicular to the hot-pressing direction. In all instances, longer cracks were observed perpendicular to the hot-pressing direction than parallel to it, indicating a lower fracture toughness for this orientation. The largest effect of orientation was observed in the Si_3N_4–BN composite in which no cracks were observed emanating from the indent along the hot-pressing direction. The upper and lower K_{Ic} values listed in Table II for the monolithic Si_3N_4 and the Si_3N_4–SiC and Si_3N_4–TiC composites represent values obtained from cracks oriented parallel and perpendicular to the hot-pressing direction, respectively. The single K_{Ic} value listed for the Si_3N_4–BN composite represents cracking perpendicular to the hot-pressing direction; K_{Ic} along the hot-pressing direction is unknown since cracks were not detected in this orientation.

The results in Table II indicate that the effects of the particulate addition on mechanical properties depended on the nature of the particulate. The 20 vol % addition of SiC to Si_3N_4 resulted in increased hardness, flexural strength, fracture toughness, and Young's modulus. The 20 vol % addition of TiC resulted in increased hardness and flexural strength and decreased fracture toughness and Young's modulus. The 20 vol % addition of BN resulted in decreased hardness, flexural strength, fracture toughness, and Young's modulus.

3.2. Contact damage resistance

Coefficient of friction (μ_f) values obtained from the friction and wear experiments are shown in Fig. 2. Condition No. 1 represents the single-stroke test as previously described. The static (breakaway) and dynamic coefficients of friction are plotted for each material and were determined by averaging the results obtained during single-stroke tests of two separate specimens. It is evident from the data that the Si_3N_4–TiC composite exhibited the highest values for the static and dynamic coefficient of friction, and the Si_3N_4–SiC composite exhibited the lowest values. No general trend was observed between the static and dynamic coefficients of friction for each material. The Si_3N_4–TiC composite exhibited the highest static coefficient of friction of 0.63 and showed a decrease to a dynamic coefficient of friction of 0.49. This was possibly due to the formation of an oxide layer causing some initial sticking and subsequent lubrication,

TABLE I Friction and wear test conditions

Test condition No.	Test type	Normal load (N)	Relative velocity (cm sec^{-1})	Test duration
1	Single stroke	4.9	–	1 stroke
2	Oscillatory	4.9	8	15 min (~ 3600 strokes)
3	Oscillatory	14.7	8	1 min (~ 240 strokes)

TABLE II As-fabricated material properties

Material	Density (% of theoretical)	Hardness (GPa)	Flexural strength (MPa)	Fracture toughness (MPa $m^{1/2}$)	Young's modulus (GPa)
Si_3N_4	96.1	16.7	455	4.6 to 5.9	307
Si_3N_4–SiC	96.9	18.3	634	5.1 to 6.8	326
Si_3N_4–TiC	95.5	20.5	514	4.4 to 5.2	273
Si_3N_4–BN	94.3	9.9	335	3.1	215

as discussed later. The Si_3N_4–BN and Si_3N_4–SiC composites had a higher dynamic than static coefficient of friction while the monolithic Si_3N_4 had a higher static than dynamic coefficient of friction.

Coefficient of friction values for Conditions 2 and 3, which represent the oscillating tests at low and high loads, respectively, were obtained by averaging the results of from two to four samples. In both conditions, a dramatic difference in the coefficient of friction was observed between the Si_3N_4–TiC composite and the three other materials tested. Specifically, Condition No. 2 resulted in an average coefficient of friction for the Si_3N_4–TiC composite of 0.38 while the others ranged from 0.58 to 0.69, and for Condition No. 3 a coefficient of friction of 0.38 was obtained from the Si_3N_4–TiC composite while the others ranged from 0.55 to 0.66. Ranking of the other three materials showed that the Si_3N_4–SiC composite had the highest coefficient of friction at 0.69, while the Si_3N_4–BN composite and the monolithic Si_3N_4 remained lower at between 0.58 and 0.62.

It is apparent from a comparison of the data obtained at 4.9 and 14.7 N that the coefficient of friction of each of the materials was independent of normal load, over the load range investigated. Comparison of the dynamic coefficient of friction values obtained from the single-stroke experiments (Condition No. 1) with the corresponding coefficient of friction values obtained from the reciprocating experiments (Conditions 2 and 3) suggests the presence of a time dependency in the coefficient of friction. For the Si_3N_4–SiC and Si_3N_4–BN composites and the monolithic Si_3N_4, the dynamic coefficient of friction measured during reciprocating tests, which represents the steady-state condition, was significantly higher than the dynamic coefficient of friction measured during the single-stroke experiment, which represents the initial or transient condition. The Si_3N_4–TiC composite, on the other hand, exhibited a steady-state coefficient of friction which was lower than the dynamic coefficient of friction obtained in the single-stroke tests.

Fig. 3 plots the data resulting from the four-point bend tests and compares baseline strengths to residual strengths after friction and wear testing. In addition to the average bend strengths, the maximum and minimum values of each data set are included to illustrate the true spread in the data. The effect of the wear track on residual bend strength showed considerable variation with no apparent systematic dependence on either the material or the wear conditions. The majority of the wear specimens exhibited residual bend strengths which fell well within the scatter bands obtained for the as-hot-pressed conditions. Occasional specimens, however, had bend strengths which were considerably below the as-hot-pressed scatter bands. The overall effect of this (observed in seven of the twelve material/wear conditions investigated) was a significant drop in the average strength. The residual bend strengths of

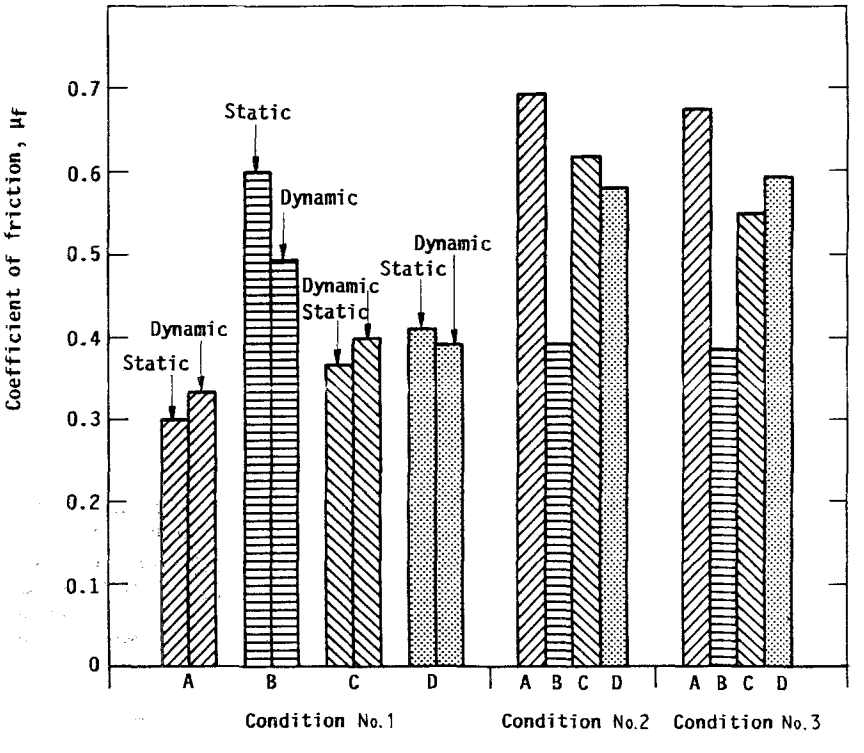

Figure 2 Comparison of the coefficients of friction for each material and testing condition. (A) Si_3N_4–SiC, (B) Si_3N_4–TiC, (C) SI_3N_4–BN, (D) Si_3N_4.

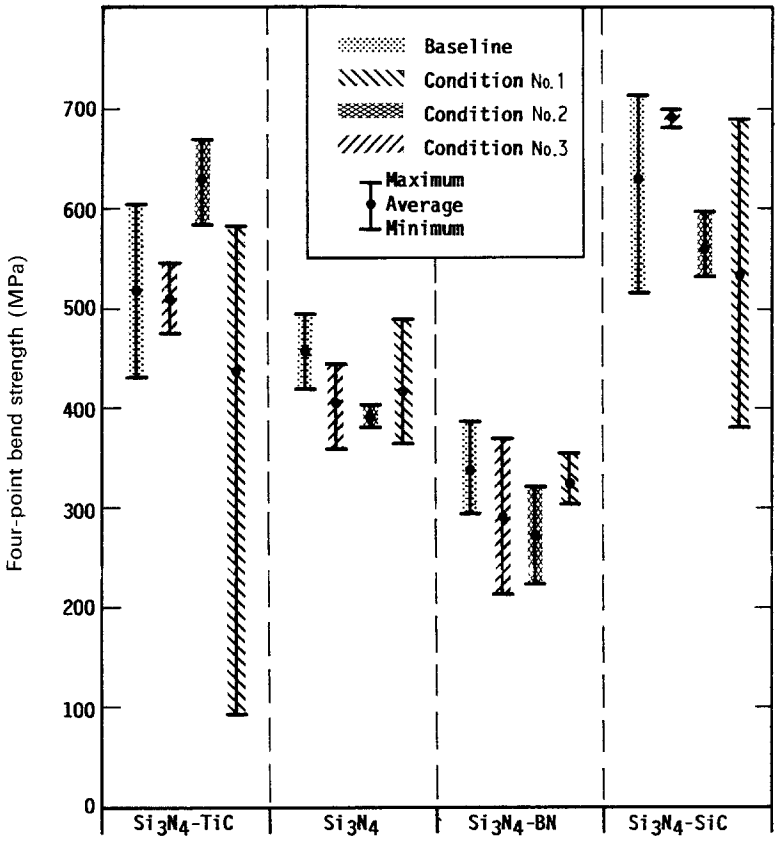

Figure 3 Comparison of baseline four-point bend strengths to residual bend strengths of worn specimens.

all of the specimens in five of the twelve material/wear conditions, however, fell entirely within or above the as-hot-pressed scatter bands.

Following the bend tests, profilometry was employed to characterize the wear tracks produced during the multipass wear tests. Typical profilometer traces for each of the materials are illustrated in Fig. 4. Average wear track depths and widths obtained from profilometer traces are listed in Table III. It is apparent from these data that large amounts of the monolithic Si_3N_4 and the Si_3N_4–SiC and Si_3N_4–BN composites were removed during the multipass wear, resulting in wide and deep wear tracks. On the other hand, the profilometer traces failed to identify any measurable removal of material during multipass wear of the Si_3N_4–TiC composite; the only evidence of the existence of a wear track in the traces was a reduction in the surface roughness. Estimates of the surface finish from the profilometer traces indicated an r.m.s. surface finish of approximately 0.50 μm outside the wear track and 0.15 μm inside the wear track.

Scanning electron microscopy was used to identify interesting features of the wear track and unworn surface on one specimen of each material tested under Condition No. 2. Examination of the unworn surface

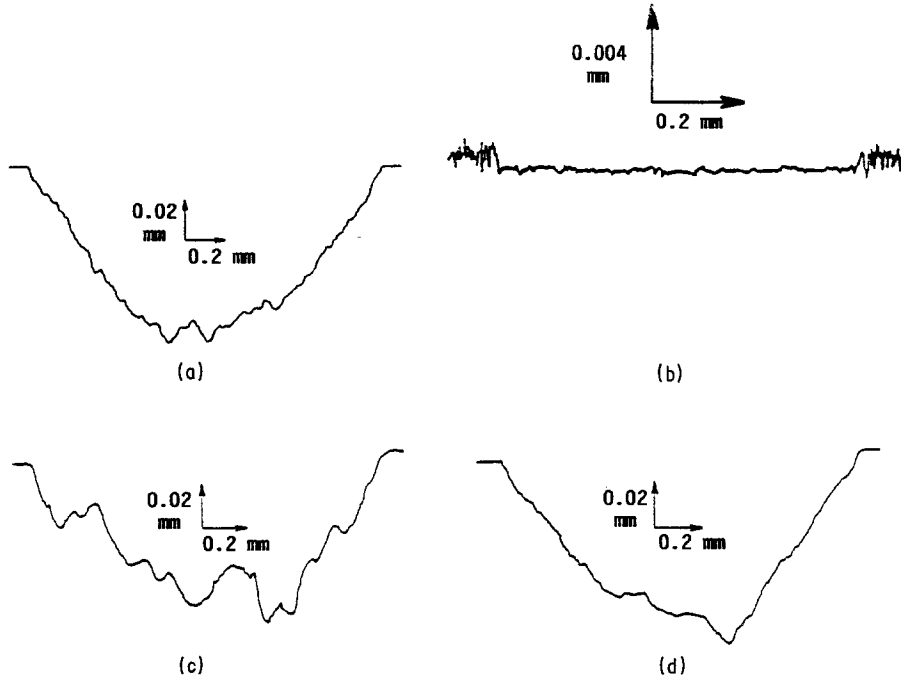

Figure 4 Profilometer results for each material after a multi-stroke test showing the polished surface of the Si_3N_4–TiC composite and the worn surfaces of the remaining materials. (a) Si_3N_4–SiC, (b) Si_3N_4–TiC, (c) Si_3N_4–BN, (d) Si_3N_4. Note the increased scale factor on the Si_3N_4–TiC trace.

TABLE III Wear track measurements

Wear conditions	Material	Depth of track (μm)	Width of track (μm)
4.9 N, 15 min	Si_3N_4–TiC	< 0.5	440
	Si_3N_4	57	1330
	Si_3N_4–BN	84	1690
	Si_3N_4–SiC	100	1970
14.7 N, 1 min	Si_3N_4–TiC	< 0.5	600
	Si_3N_4	40	1120
	Si_3N_4–BN	23	750
	Si_3N_4–SiC	42	1170

of the Si_3N_4–TiC composite (Fig. 5) indicated that particulate matter (light area of photo) was protruding from the surface of the Si_3N_4 (dark area of photo). Auger analysis (described below) identified these protrusions as an oxide that had developed above the TiC particles. Similar oxide protrusions were not observed on the other three materials. Comparison of the wear tracks (Fig. 5), identified additional differences between the materials. The wear track of the monolithic Si_3N_4, which is also characteristic of the Si_3N_4–SiC and Si_3N_4–BN materials, exhibited significant surface roughening, whereas the wear track of the Si_3N_4–TiC composite exhibited a polished appearance. A micrograph of the edge of the wear track of the Si_3N_4–TiC composite is presented in Fig. 6. The smeared nature of the oxide film in the wear track is evident from the micrograph.

3.3. Crack morphology

A specimen of each material (tested under Condition No. 2) was sectioned and polished parallel to the wear track in order to characterize any cracking which had occurred underneath the wear track. The presence of subsurface cracking was apparent in these cross sections (Fig. 7). Typically, the cracks ranged in depth from 10 to 50 μm. Each of the four materials exhibited cracking beneath the wear track; however, the crack density was lowest in the Si_3N_4–BN material. The majority of the cracks observed had propagated through a more or less hemispherical trajectory and either reconnected with the surface, resulting in material removal similar to that involved in delamination, or were arrested at the bottom of the trajectory, resulting in a crack tip lying parallel to the specimen surface.

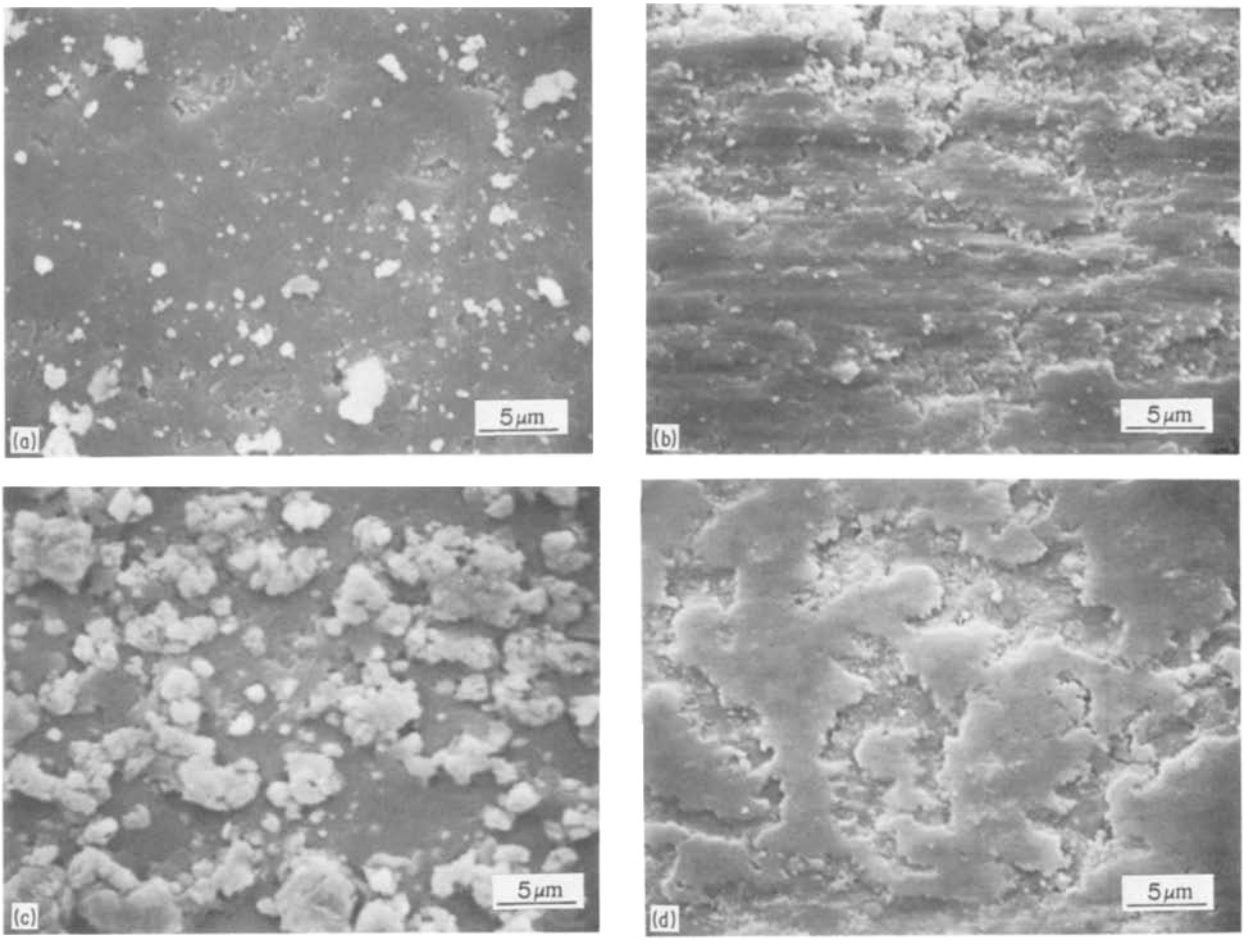

Figure 5 Scanning electron micrographs comparing the post-test surfaces of the monolithic Si_3N_4 (a) outside and (b) inside the wear track; and with Si_3N_4–TiC composite (c) outside and (d) inside the wear track.

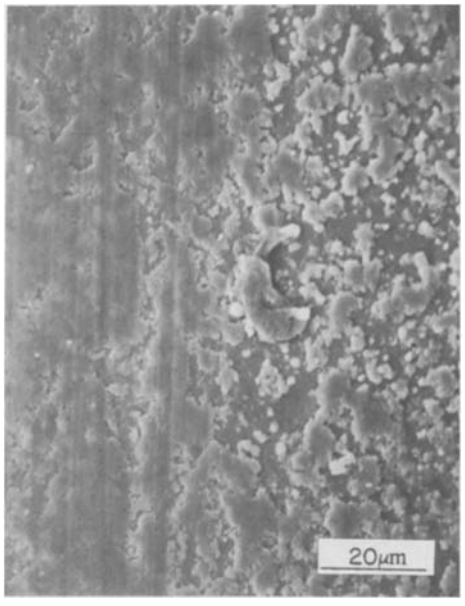

Figure 6 Scanning electron micrograph of the wear track boundary illustrating the transition from a smeared oxide lubricating layer in the wear track to a protruding oxide outside the wear track.

3.4. Auger analysis

Auger analysis was performed on one of the Si_3N_4–TiC wear samples (Condition No. 2) to help identify possible reasons for the lower coefficient of friction and much shallower wear track exhibited by that material. Spectra were obtained using a primary beam energy of 3 kV, a beam current of approximately 5×10^{-9} A, a beam size of 150 nm, and a peak-to-peak modulation voltage of 2 V. Elemental depth profiles were also obtained at various points on the wear track using an ion-beam voltage of 2 kV, and a current density of 33 μA cm^{-2} rastered over a 2 mm × 2 mm area. The sputter conditions corresponded to a sputter rate of approximately 6 nm min^{-1} as measured on a Ta_2O_5 standard.

Examination of the wear track using secondary electron microscopy identified the presence of two distinct regions: a continuous phase which corresponded with the underlying Si_3N_4 matrix, and a discontinuous phase which corresponded with the underlying TiC particles. Auger spectra (Figs 8a and 9a) show the presence of carbon, nitrogen, oxygen and titanium on the surface of both of these regions. The presence of nitrogen is deduced from the unusually large peak-height relationship between the two titanium *LMM* peaks at 387 and 418 eV. Elemental titanium has a peak height (PH) ratio PH(387)/PH(418) < 1. Under the present friction and wear test conditions, titanium is expected to be in an oxidized form. Oxidation of titanium causes changes in the Auger spectra including a change in the peak height ratio PH(387)/PH(418) to slightly greater than unity. The peak height ratios observed in Figs 8a and 9a are much larger than expected for oxidized titanium, and are considered to be due to the overlap of the nitrogen *KLL* peak at 379 eV with the titanium 387 eV peak.

Elemental depth profiling shows that the carbon

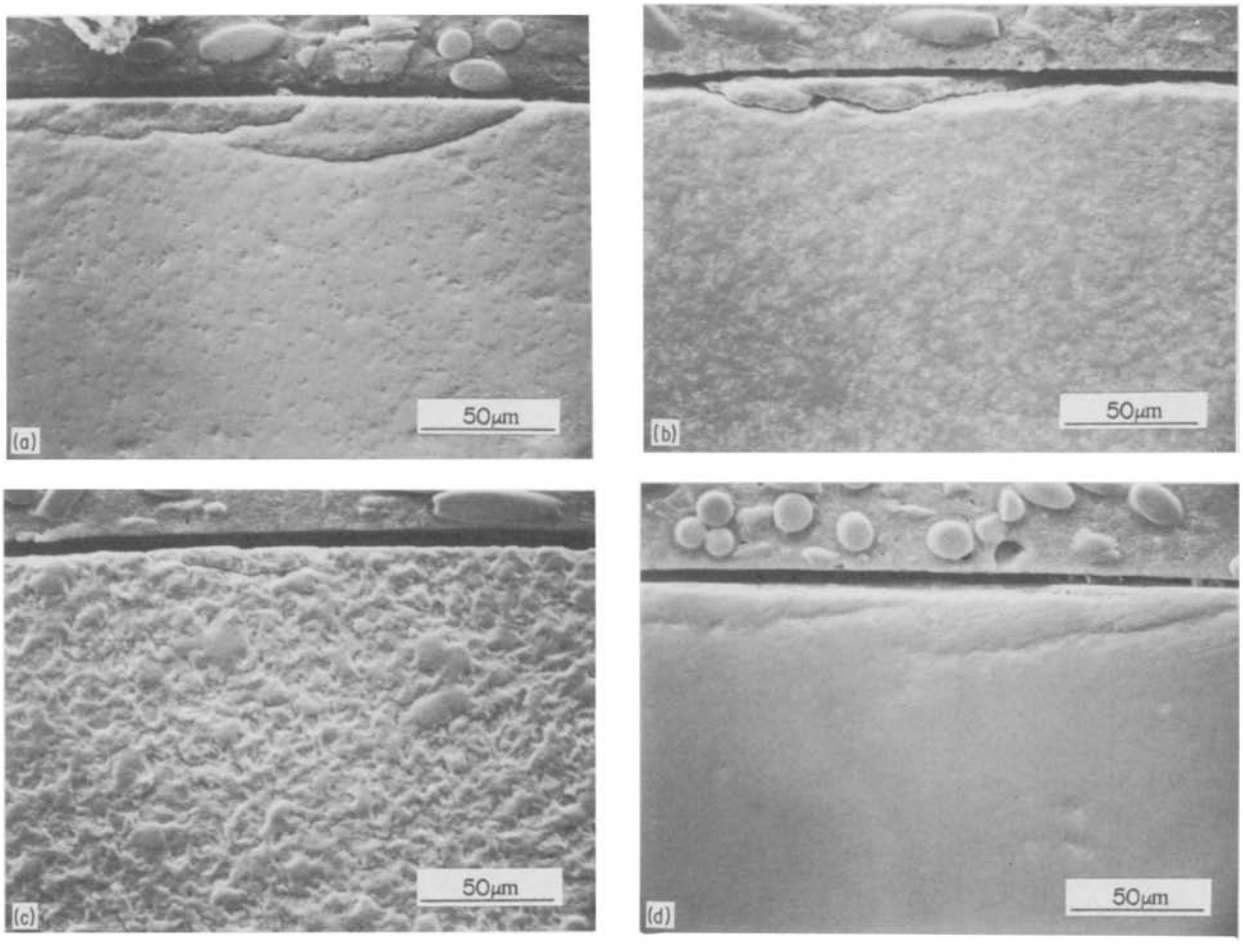

Figure 7 Cross-sections through multi-stroke wear tracks of (a) Si_3N_4–SiC, (b) Si_3N_4–TiC and (c) Si_3N_4–BN composites, and (d) monolithic Si_3N_4, illustrating the crack geometry present beneath the track.

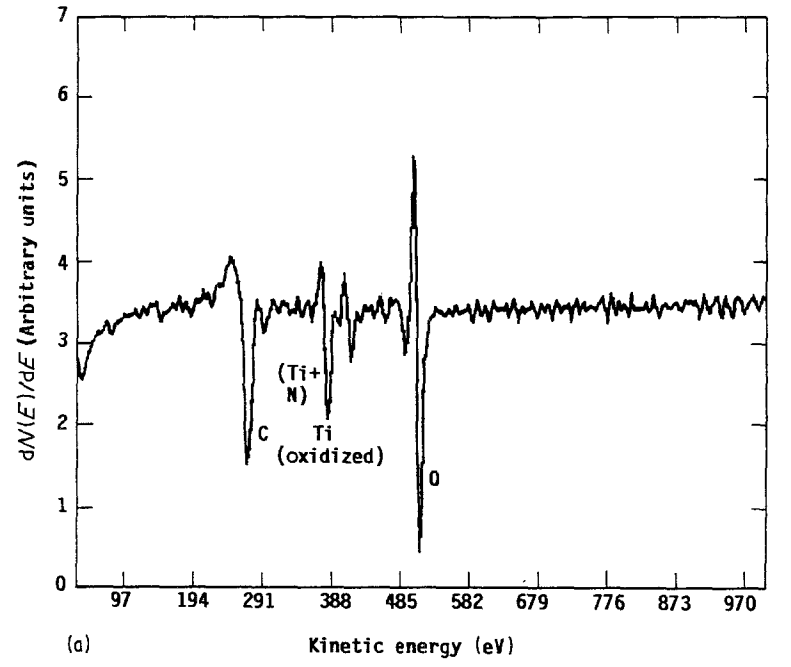

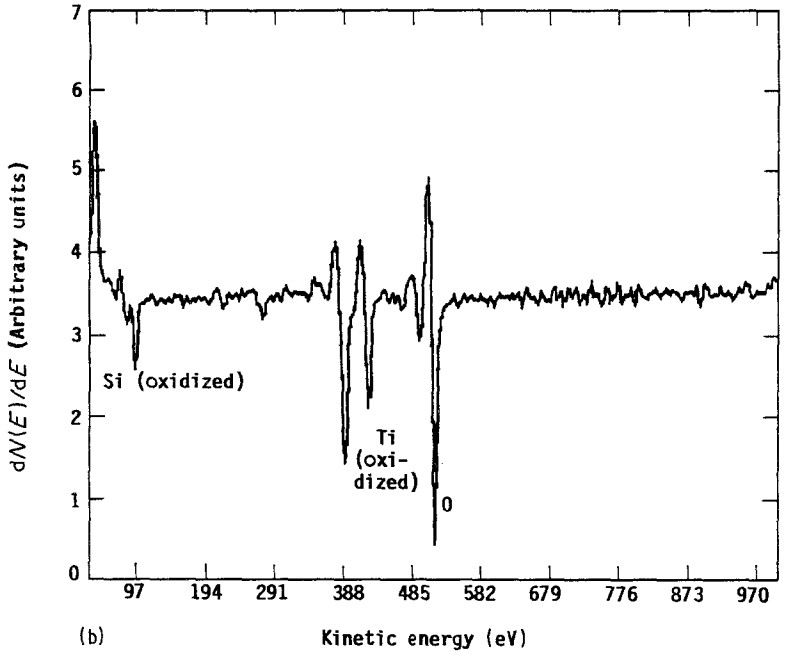

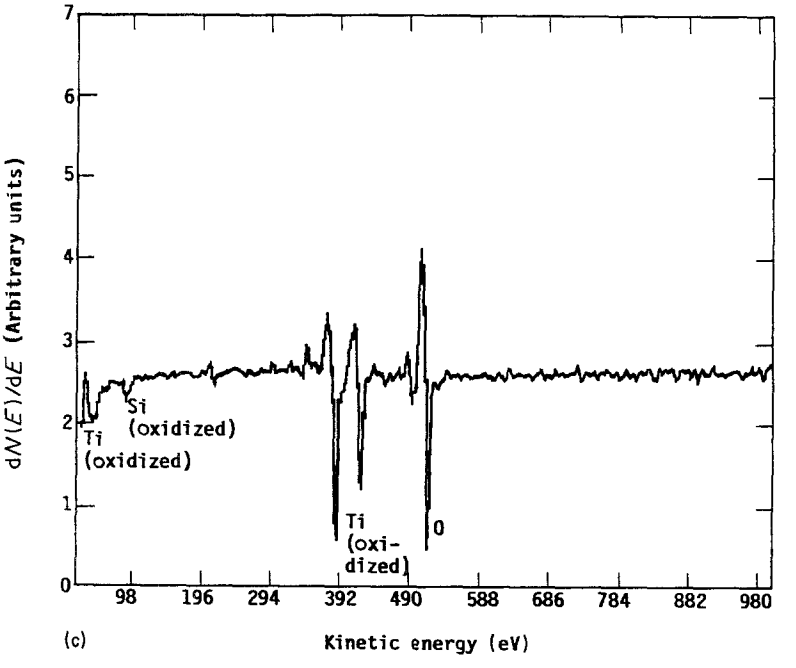

Figure 8 Auger spectra obtained over a TiC particle in the wear track of an Si_3N_4–TiC composite (a) prior to sputtering, (b) after 1 min of sputtering and (c) after 20 min of sputtering.

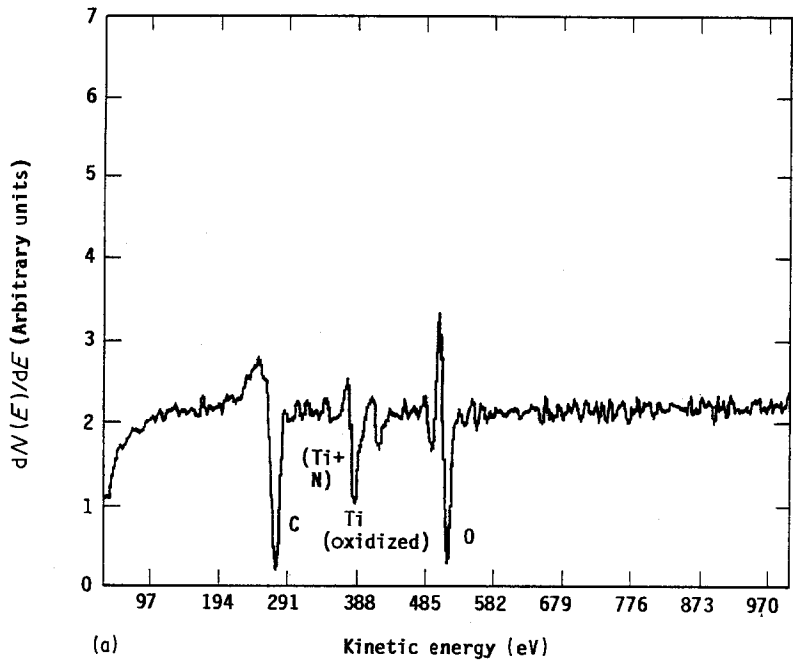

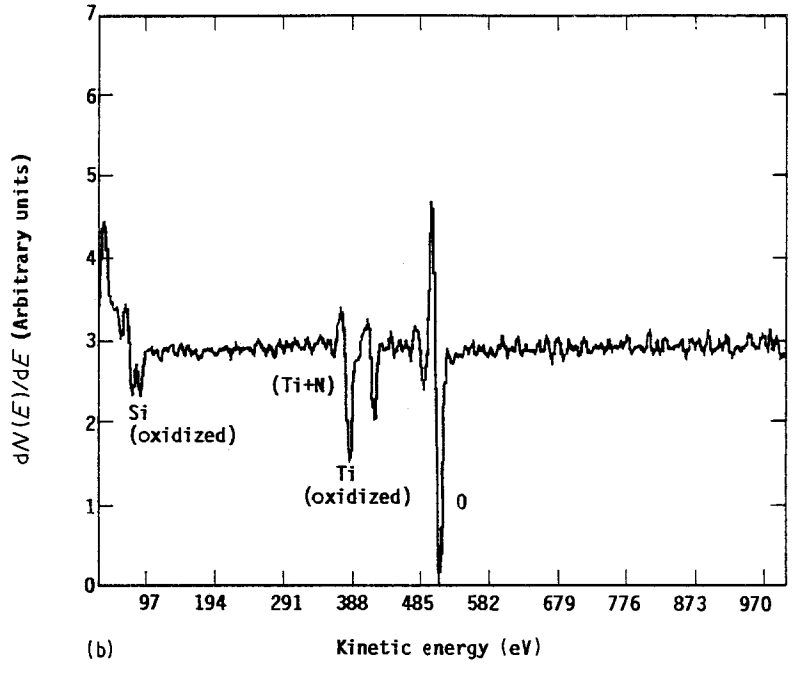

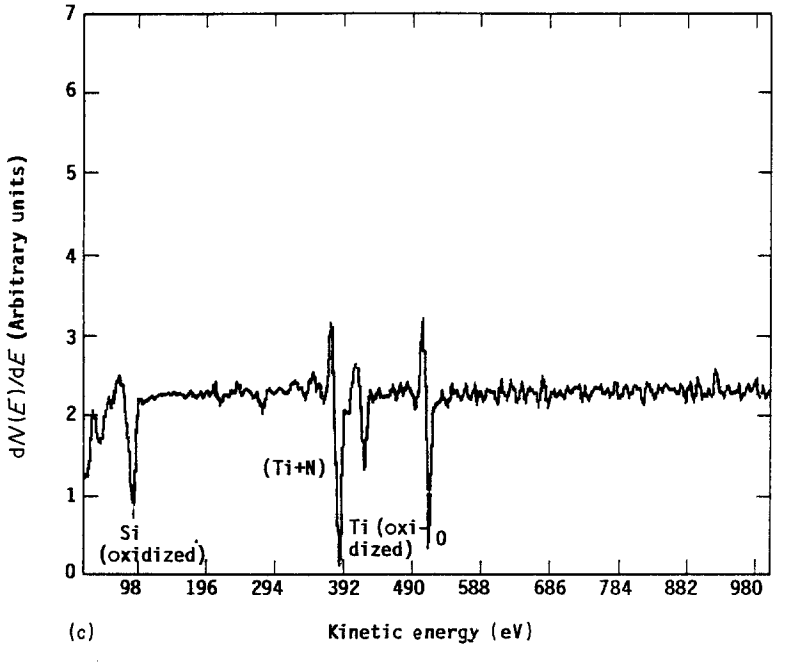

Figure 9 Auger spectra obtained over the Si_3N_4 matrix in the wear track of an Si_3N_4–TiC composite (a) prior to sputtering, (b) after 1 min of sputtering and (c) after 20 min of sputtering.

was probably present as surface contamination, as it was removed after one minute of sputtering (Figs 8b and 9b). In addition, the presence of silicon, probably in the oxidized form, was observed over both regions. Further sputtering for up to 20 min produced a reduction in the silicon signal with respect to the titanium peaks over the dark phase, the TiC particles (Fig. 8c). On the other hand, the silicon peak increased in size relative to the titanium peaks over the Si_3N_4 matrix, and the nitrogen signal (overlapping the titanium 387 eV peak) became much stronger (Fig. 9c). In all of the Auger spectra, silicon is probably in the oxide state, and perhaps the nitride or carbide state (in the case of the pin to be discussed). Electron-beam decomposition effects and preferential sputtering do not allow a distinction between these states, but the elemental state, which might be inferred from the spectra of Figs 8c, 9b, 9c, 10a and 10b, is not expected.

The SiC pin run against this particular flat was also examined with secondary and Auger electron microscopy. In order to avoid charging problems associated with a small, non-conducting specimen, the wear surface was observed at a glancing angle. Therefore, the depth profiling conditions given for the flat specimen do not apply in this case.

Secondary electron microscopy of the pin indicated the presence of a burnished-appearing region. Auger spectra from this region (Fig. 10a) indicated that the surface contained carbon, nitrogen, silicon in an oxidized form, and titanium. After five minutes of sputtering (at glancing angle), the spectra showed that carbon had been removed, while signals for oxygen, silicon and titanium remained (Fig. 10b). Comparison of the spectra obtained from the SiC pin (Fig. 10) with those obtained from the wear track (Figs 8 and 9) indicates that a similar surface layer was present on both. Since the composite wear specimen was the only possible source of nitrogen and titanium, it can be concluded that the surface layer observed on the SiC pin was a deposit made up of oxidized constituents from the Si_3N_4–TiC wear specimen.

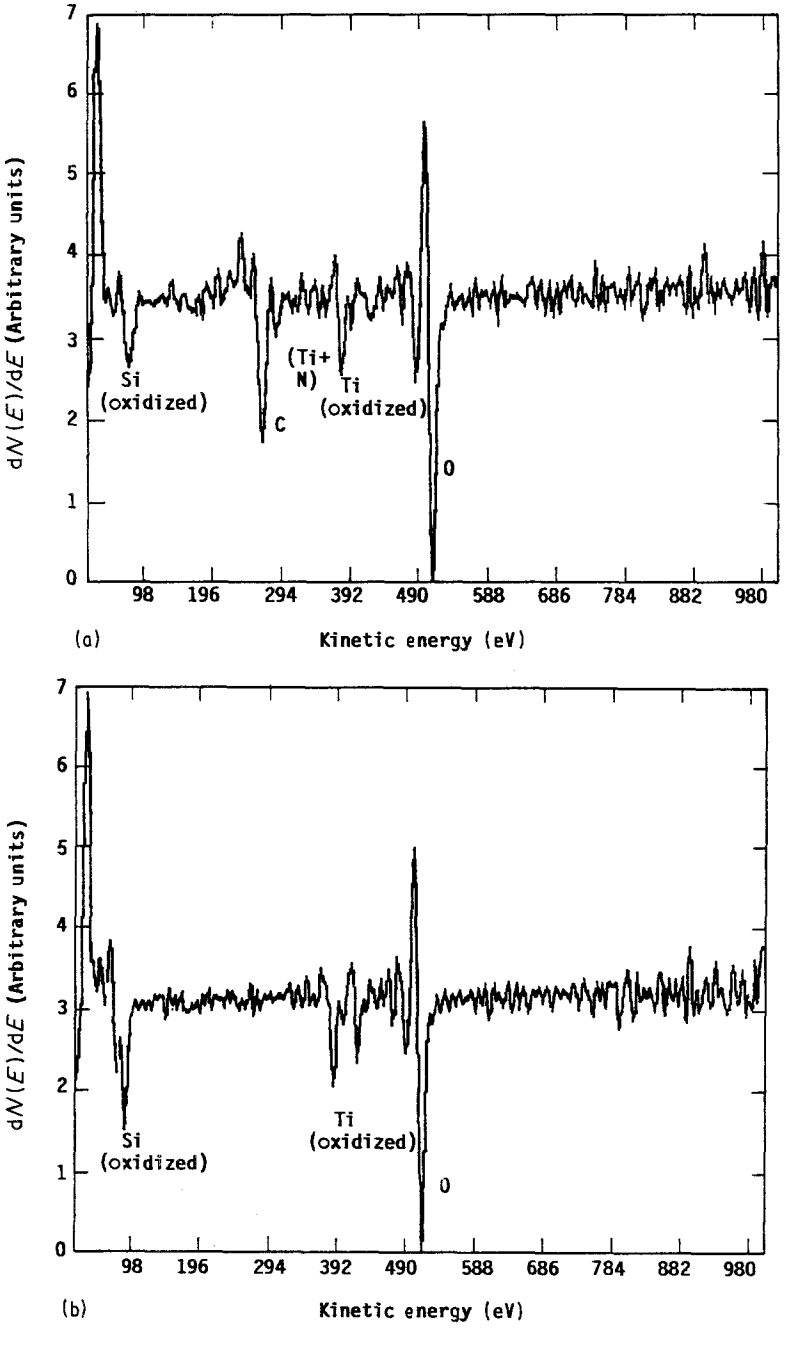

Figure 10 Auger spectra from SiC pin employed for wear test of Si_3N_4–TiC specimen (a) prior to sputtering and (b) after 5 min of sputtering.

4. Discussion

A major form of damage which can occur during sliding contact of brittle materials is the formation of partial cone cracks at the trailing edge of the sliding indenter. Cracking initiates at the trailing edge because of the enhanced stresses which exist at this location [11]. The maximum tensile stress experienced during sliding contact, σ_m, is given [11] by

$$\sigma_m = (1 + 15.5\mu_f)(\tfrac{1}{2} - \nu)\frac{P}{\pi a^2} \quad (3)$$

where μ_f is the coefficient of friction, ν is Poisson's ratio, P is the normal load applied to the indenter and a is the radius of the contact area. The value of a is obtained from

$$a^3 = \frac{4}{3}\frac{kPr}{E} \quad (4)$$

where r is the indenter radius, E is Young's modulus and k is defined by

$$k = \frac{9}{16}\left[(1 - \nu^2) + \left(\frac{E}{E_i}\right)(1 - \nu_i^2)\right] \quad (5)$$

The subscript i in Equation 5 signifies the indenter material. Using the above equations, the maximum tensile stresses experienced during the wear tests reported in this study are estimated to be on the order of 1000 to 1700 MPa for the indenter load of 4.9 N, and 1450 to 2400 MPa for the indenter load of 14.7 N. Since the maximum stresses, even for the low indenter load, greatly exceed the bending strengths measured for the four materials of this study, the formation of partial cone cracks would be expected.

Sliding contact tests performed on reaction-bonded Si_3N_4 by Richerson *et al.* [11], which yielded similar maximum stress values, were found to produce partial cone cracks and a subsequent drop in residual bend strength. A similar reduction in flexural strength was generally not observed for the materials and conditions employed in this study; only occasionally were the bend strengths found to be dramatically reduced by the wear track. The cross-sections through the wear tracks indicated that cracking had occurred. However, the geometry of the cracks were similar to the lateral cracks which are formed by the residual stresses developed during load removal [14] or the delamination cracks which result from plastic deformation of the substrate [15], rather than the partial cone cracks which form under load as the direct result of σ_m. Because of their geometry, the cracks observed in the wear track are much less likely to result in a reduction in bend strength than are partial cone cracks, which extend into the substrate at higher angles to the tensile direction during bending.

An explanation for the absence of partial cone cracking may lie in the ability of the substrate to deform plastically under the indenter. The calculations of σ_m presented above assume completely elastic behaviour. The presence of any plastic deformation under the indenter would act to reduce the actual stresses and thus inhibit cracking. Adewoye and Page [16] have observed plastic deformation accompanied by delamination during the wear of silicon nitrides at room temperature. The elevated temperatures employed in this work would be expected to further enhance plasticity.

Although a correlation between residual bend strength and wear behaviour was not observed, a strong correlation between wear behaviour and the coefficient of friction was. The monolithic Si_3N_4 and the Si_3N_4–SiC and Si_3N_4–BN composites exhibited dynamic coefficients of friction which were initially low and increased to their steady-state values, while the Si_3N_4–TiC composite exhibited a dynamic coefficient of friction that was initially high and decreased to its steady-state value. Breznak *et al.* [17] have found that a coefficient of friction that increases to its steady-state value indicates roughening of the wear track, while one that decreases to its steady-state value indicates smoothing. A similar correlation was exhibited by the materials employed in this study. The profilometer traces indicated that roughening occurred in the monolithic Si_3N_4 and the Si_3N_4–SiC and Si_3N_4–BN composites, while smoothing of the surface finish occurred in the Si_3N_4–TiC composite. This effect may also be observed in Fig. 5 where the Si_3N_4–TiC composite exhibited a polished surface in contrast to the roughened surface finish of the monolithic Si_3N_4 wear track. The surface roughening which took place in the Si_3N_4, Si_3N_4–SiC and Si_3N_4–BN materials led to high wear rates and the formation of a pronounced wear track, while the surface smoothing which took place in the Si_3N_4–TiC material resulted in negligible wear rates.

Previous studies of ceramic wear have found that coefficients of friction and wear rates were reduced when testing was performed in an oxidizing rather than an inert environment [18–20]. Analysis of the surfaces produced in oxidizing environments has shown that the formation of a thin oxide layer during wear is responsible for the improvement in wear resistance [18–22]. Apparently, the oxide layer provides a type of solid (or quasi-liquid, at friction-induced locally elevated temperatures) lubrication between the ceramic surfaces. Available data [23–27] also suggest that titanium oxide is one of the more proficient oxides at reducing μ_f and increasing wear resistance.

Using the above results, it is possible to rationalize the improved friction and wear behaviour observed with the addition of TiC particles. Auger analysis of the wear track has shown that the TiC particles exposed at the surface had oxidized and that the titanium oxide had smeared over the entire wear track, being found both above the TiC particles and the Si_3N_4 matrix. Silicon oxide was also found in the surface film. The presence of silicon oxide may be a significant factor in the friction and wear behaviour since a low melting point eutectic exists in the SiO_2–TiO_2 phase diagram [28]. Additionally, an oxide film containing both titanium, which could only have come from the wear track, and silicon was also found on the SiC rider. Thus, the SiC hemisphere was riding on a continuous film of lubricious oxide containing both titanium and silicon, the presence of which has been shown [26, 27] to dramatically improve wear behaviour. Since the TiC particles were the only

source of titanium in either the ceramic substrate or the rider, the presence of the beneficial titanium oxide film and the corresponding improvement in wear behaviour would not be expected in any of the other substrate materials.

It is clear from the results of this study that the addition of TiC particles provided greatly enhanced wear resistance in a high-temperature oxidizing environment compared to that exhibited by the Si_3N_4 matrix alone. The improved wear resistance was due to the formation of a lubricious oxide film that was composed of a mixture of titanium and silicon oxides. The addition of SiC particles, which were found to improve both the flexural strength and fracture toughness, or BN particles, which are lubricious at lower temperatures, provided no measurable improvement in the wear resistance. The lack of an improvement with the SiC particles suggests that flexural strength and fracture toughness, both of which were increased by the SiC particulate addition, did not play a primary role in determining wear behaviour under the conditions employed in the study. Rather, the primary controlling variable appeared to be the frictional behaviour of the surface oxide that formed during wear in the oxidizing environment. These results suggest that future attempts to improve wear behaviour in these types of system should emphasize improvements in the lubricating nature of the surface films, rather than improvements in the resistance to fracture.

5. Conclusions

The following conclusions can be drawn from the results obtained in this investigation.

1. The addition of TiC particles to an Si_3N_4 matrix produced greatly improved friction and wear behaviour. The observed improvement was due to the formation of a lubricious film containing oxides of both silicon and titanium between the rider and the substrate.

2. The addition of SiC particles to an Si_3N_4 matrix produced improved bend strength and fracture toughness but failed to impart any improvement in the friction and wear behaviour.

3. The addition of BN particles to an Si_3N_4 matrix improved neither the bend strength and fracture toughness nor the friction and wear behaviour.

4. Cracking along the wear tracks was similar in geometry to the lateral cracking under indents or the cracking accompanying delamination. The geometry of the cracking led to cracks which did not generally produce any decrease in residual bend strength.

Acknowledgements

This research was sponsored by the Internal Research Program of Southwest Research Institute. The assistance of Messrs D. N. Weed and J. L. Sievert is also gratefully acknowledged.

References

1. D. W. RICHERSON and K. M. JOHANSEN, "Ceramic Gas Turbine Engine Demonstration Program", Garret Final Report, Contract No. N00024-76-C5352, (Garret, 1982).
2. R. W. RICE, "An Assessment of the Use of Ceramics in Heat Engines", NRL Memorandum Report 4499 (NRL, 1981).
3. C. A. ANDERSON, "Ceramic Turbine Components Research and Development; Part 1–Ceramic Rotor-Blade Development", Final Report, EPRI Project No. AP-1539 (EPRI, 1980).
4. B. R. LAWN and M. V. SWAIN, *J. Mater. Sci.* **10** (1975) 113.
5. B. R. LAWN and E. R. FULLER, *ibid.* **10** (1975) 2016.
6. B. R. LAWN and R. WILSHAW, *ibid.* **10** (1975) 1049.
7. C. M. PERROTT, *Wear* **45** (1977) 293.
8. A. G. EVANS and E. A. CHARLES, *J. Amer. Ceram. Soc.* **59** (1976) 371.
9. P. CHANTIKUL, G. R. AUSTIS, B. R. LAWN and D. B. MARSHALL, *ibid.* **64** (1981) 539.
10. B. R. LAWN, *Proc. R. Soc.* **A299** (1967) 307.
11. D. W. RICHERSON, D. G. FINGER and J. M. WIMMER, in "Fracture Mechanics of Ceramics", Vol. 5 edited by R. C. Bradt, A. G. Evans, D. P. H. Hassleman and F. F. Lange (Plenum, New York, 1983) pp. 163–184.
12. D. R. GILROY and W. HIRST, *Br. J. Appl. Phys.* **2** (1969) 1784.
13. K. S. MAZDIYASNI and R. RUH, *J. Amer. Ceram. Soc.* **64** (1981) 415.
14. B. R. LAWN, M. V. SWAIN and K. PHILLIPS, *J. Mater. Sci.* **10** (1975) 1236.
15. N. SUH, *Wear* **25** (1973) 111.
16. O. O. ADEWOYE and T. F. PAGE, *ibid.* **70** (1981) 37.
17. J. BREZNAK, E. BREVAL and N. H. MacMILLAN, *J. Mater. Sci.* **20** (1985) 4657.
18. D. J. BARNES and B. D. POWELL, *Wear* **32** (1975) 195.
19. P. SUTOR, in Proceedings of 9th Annual Conference on Composites and Advanced Ceramic Materials, (American Ceramic Society, Columbus, Ohio, 1985) pp. 460–469.
20. T. E. FISCHER and H. TOMIZAWA, *Wear* **105** (1985) 29.
21. R. P. STEIJN, *ibid.* **7** (1964) 48.
22. H. SHIMURA and Y. TSUYA, in Proceedings of International Conference on Wear of Materials (ASME, New York, 1977) pp. 452–461.
23. D. J. BOES, in Proceedings of 22nd Contractors Coordinating Meeting (Society of Automotive Engineers, Warrendale, Pennsylvania, 1984) p. 323.
24. L. B. SIBLEY and C. M. ALLEN, *Wear* **5** (1962) 312.
25. S. GRAY, in Proceedings of 9th Annual Conference on Composites and Advanced Ceramic Materials (American Ceramic Society, Columbus, Ohio, 1985) pp. 965–975.
26. J. LANKFORD, W. WEI and R. KOSSOWSKY, *J. Mater. Sci.* **22** (1987) 2069.
27. W. WEI and J. LANKFORD, *ibid.* **22** (1987) 2387.
28. E. M. LEVIN, H. F. McMURDIE and F. P. HALL, "Phase Diagrams for Ceramists" (American Ceramic Society, Columbus, Ohio, 1956) p. 66.

Received 7 April
and accepted 23 June 1987